Article

Developing Comprehensive Local Climate Zone Land Use Datasets for Advanced High-Resolution Urban Climate and Environmental Modeling

Yongwei Wang [1,*] **, Danmeng Zhao** [1] **and Qian Ma** [2]

1   School of Atmospheric Physics, Nanjing University of Information Science and Technology,
    Nanjing 210044, China; 20211203037@nuist.edu.cn
2   Wenzhou Meteorological Bureau, Wenzhou 325000, China; maqiana246306@cma.cn
*   Correspondence: wyw@nuist.edu.cn

Abstract: The Local Climate Zone (LCZ) classification scheme is a vital method of building a category dataset for high-resolution urban land. For the development of urban meteorology, air pollution and related disciplines, the high-resolution classification data of urban buildings are very important. This study aims to create LCZ datasets with detailed architectural characteristics for major cities and urban agglomerations in China, and obtain more accurate results. We constructed 120 m resolution land use datasets for 63 cities (mainly provincial capitals, municipalities directly under the Central Government, important prefecture-level cities and special administrative regions) and 4 urban agglomerations in China based on the local climate zone (LCZ) classification scheme using the World Urban Database and Access Portal Tools method (WUDAPT). Nearly 100,000 samples were used, of which 76,000 training samples were used to provide spectral signatures and 23,000 validation samples were used to ensure accuracy assessments. Compared with similar studies, the LCZ datasets in this paper were generally of good quality, with an overall accuracy of 71–93% (mean 82%), an accuracy for built classifications of 57–83% (mean 72%), and an accuracy for natural classifications of 70–99% (mean 90%). In addition, 35% of 63 Chinese cities have construction areas of more than 5%, and the plateaus northwest of Chengdu and Chongqing are covered with snow all year round. Therefore, based on the original LCZ classification system, the construction area (LZC H) and the snow cover (LCZ I) were newly added as the basic classifications of urban LCZ classification in China. Detailed architectural features of cities and urban agglomerations in China are provided by the LCZ datasets in this study. It can be applied to fine numerical models of the meteorological and atmospheric environment and improve the prediction accuracy.

Keywords: local climate zone; WUDAPT method; land use datasets; urban climate simulation

1. Introduction

As an important input condition of numerical models, land use data affects the simulation of meteorological factors, and further affects the simulation of transport, diffusion, formation and the removal of pollutants [1]. Different land use classifications have different release properties of sensible heat and latent heat due to differences in the surface physical parameters, which affect the land surface energy balance [2]. They also affect the dynamic and thermal interaction of the atmospheric boundary layer, resulting in changes in temperature, humidity and precipitation within the boundary layer [3–5]. Changes in the simulation results of meteorological factors affect the simulation results for transport and the diffusion of air pollutants [6,7]. The simulation of spatial and temporal variations in pollutants is significantly affected by the accuracy of land use data. The accuracy of pollutant concentration simulation can be effectively improved by using high-precision land use data [8–11]. The model's ability to express urban land surface processes can be improved, and the prediction accuracy can be further improved by applying high-precision

land use data to model simulation, such as LCZ (Local Climate Zone) [12,13]. Existing studies have shown that LCZ can be used to simulate meteorological factors in the study area more accurately [12–17], and show that changes in meteorological conditions, such as temperature, wind speed and humidity, have a significant impact on the transport and diffusion of pollutants, as well as the chemical reaction process [2,15].

The existing land use data used in urban meteorological and environmental simulation are still insufficient. At present, the simulation of the urban climate and environment relies on two forms of urban land use data: (a) a wide range of regional or global two-dimensional land cover data at a resolution of tens or dozens of meters, acquired by satellite or ground-based mapping [18,19] and (b) more sophisticated urban-scale data with three-dimensional building features [20–23]. Such data have laid a useful foundation for scientific research on the sustainable development of urbanization, but shortcomings remain. On one hand, most regional- or global-scale high-resolution land use maps do not provide sufficient building details. The lack of building height, building density, street spacing, and other detailed information to describe the urban canopy means that models cannot adequately capture the surface turbulence and boundary layer characteristics of urban areas, limiting urban climate high-resolution simulations [24–26]. On the other hand, although three-dimensional building data or land use data at the urban-scale can compensate for this, there are significant spatial differences in this classification data due to different data sources, land use classification schemes, and mapping standards. This makes it impossible to compare and evaluate land policy and other related environmental policy impacts on cities [27], hindering the progress of urban climate studies [27–30]. Therefore, the establishment of consistent high-resolution urban datasets with sufficient building spatial details is particularly important for high-resolution simulations [31,32].

Local climate zone (LCZ) datasets can complement these deficiencies by considering the representation of urban architectural classification and functional zones in high-resolution data. Firstly, this classification method can capture data on a larger scale [33]. Secondly, compared with traditional land use classification methods [34], the LCZ scheme standardizes the urban form and function zoning, and provides ten classifications of more detailed classifications of buildings. This is used to classify the urban underlying surface, based on high-resolution LCZ datasets with building classifications, allowing basic parameters required by the numerical model to be obtained (such as the proportion of impervious surface, man-made heat emissions, and sky-visible factors). These parameters can be introduced into the numerical model to better describe the heterogeneity of the underlying urban surface. This improves the characterization of surface dynamic forces and thermal impacts on the atmosphere, which are very important for urban climate and atmospheric environment research [26,35]. LCZ datasets present different levels of precision, based on different fabrication methods [36–40]. The World Urban Database and Access Portal Tools (WUDAPT) method provides an operational process for producing LCZ datasets and has been widely used in some European and Asian cities [41–46]. The exiting results show that the overall accuracy rate is about 96% when the WUDAPT method is applied to areas in which buildings are relatively uniform, such as Europe [28,47]. However, further studies have found that it is difficult to obtain land use data that are similar to European cities when using the WUDAPT method in areas with more complex buildings. Therefore, when using the WUDAPT method in areas with complex building forms, it is necessary to adjust the method or use more auxiliary data [44,48–51].

For areas with complex building forms, sample data that are accurate, high quality, and representative can lead to better machine learning outcomes, which is also very important for improving the accuracy of LCZ data [47,52]. WUDAPT recommends that the number of training samples of each LCZ classification is at least 5 when using the WUDAPT method to classify LCZ [40]. Existing studies using the WUDAPT method to classify LCZ have not used many sample data [48,53,54]. The number of training samples used can obtain relatively high accuracy when the WUDAPT method is applied to areas in which buildings are relatively uniform, such as Europe; however, more samples are needed in areas with

complex building forms [55,56]. In areas with complex building forms, their specific impact has not been mentioned in the existing studies on the acquisition of LCZ datasets.

China is currently the fastest urbanizing country in the world, and LCZ data production has been conducted in some cities [55–57]; however, a large amount of city data still need to be developed based on the current needs of urban meteorology, fine-scale environmental forecasts, meteorological disaster assessments, air pollution, and so on. In addition, unlike European and American countries, there are a large number of construction areas in China that have similar properties to bare soil or sandy soil; however, there are other construction materials (such as dust nets) on the surface of the construction areas. On the plateau in the northwest of Chengdu and Chongqing, there is perennial snow cover. These two kinds of classification of land use cannot be classified using the LCZ classification defined by Oke [25]. Therefore, in this paper, two new land-use classifications were added on the basis of the original LCZ classification by Oke, which were, respectively, defined as construction area (LCZ H) and plateau snow cover area (LCZ I), so as to produce datasets that better fit the characteristics of land use in China. The more detailed land use data can improve the simulation accuracy of meteorological factors and air pollutants.

In this paper, the LCZ datasets of China are generated using the WUDAPT method, including 4 large urban agglomeration regions (Beijing–Tianjin–Hebei, BTH; Yangtze River Delta, YRD; Pearl River Delta, PRD; and Chengdu–Chongqing, CC) and 63 cities, which are mainly provincial capitals, municipalities directly under the Central Government, important prefecture-level cities and special administrative regions. The aim of this paper is to explore the following scientific questions: Firstly, whether the establishment of a large number of accurate samples, including approximately 76,000 training samples and 23,000 validation samples, can effectively improve the precision of the data. Secondly, whether the existing classification of LCZ underlying surfaces applied in China is sufficient or if there is a need for additional new classification definitions. What is the proportion of these new classification in different regions? By addressing these scientific questions, we aim to establish more accurate and comprehensive LCZ underlying surface data that are applicable to major cities and urban agglomerations in China.

2. Materials and Methodology

2.1. Study Area

The 63 Chinese cities included provincial capitals, municipalities directly under the central government, major prefecture-level cities, and special administrative regions (Figure 1). The study area (90°53′–126°54′E and 46°02′–18°11′N) spanned many climatic zones, including temperate continental, temperate monsoon, subtropical monsoon, tropical monsoon, plateau, and mountainous climatic zones. As the selected cities and urban agglomerations have different urban structures and forms, studying the transition from cities to urban agglomerations can enable a clearer understanding of the adaptability of the WUDAPT method within urban built-up areas and larger regions.

Figure 1 shows the geographical location of the study area and training samples for each LCZ classification. Figure 1a shows the geographical locations of the 63 Chinese cities (including provincial capitals, municipalities directly under the Central Government, important prefecture-level cities and special administrative regions), and the 4 urban agglomerations (Beijing–Tianjin–Hebei, BTH; Yangtze River Delta, YRD; Pearl River Delta, PRD; and Chengdu–Chongqing, CC) involved in this paper. Figure 1b–e, respectively, shows some of the training samples of each LCZ classification in BTH, YPD, PRD and CC in detail, where the base map is an lCZ classification map, on the basis of which partial samples are given. For example, the blue box in the figure represents some training samples of water, and the densely yellow-lined small areas on the map represent manually delineated samples for each region. As can be seen from the figure, a large number of training samples are used in this paper.
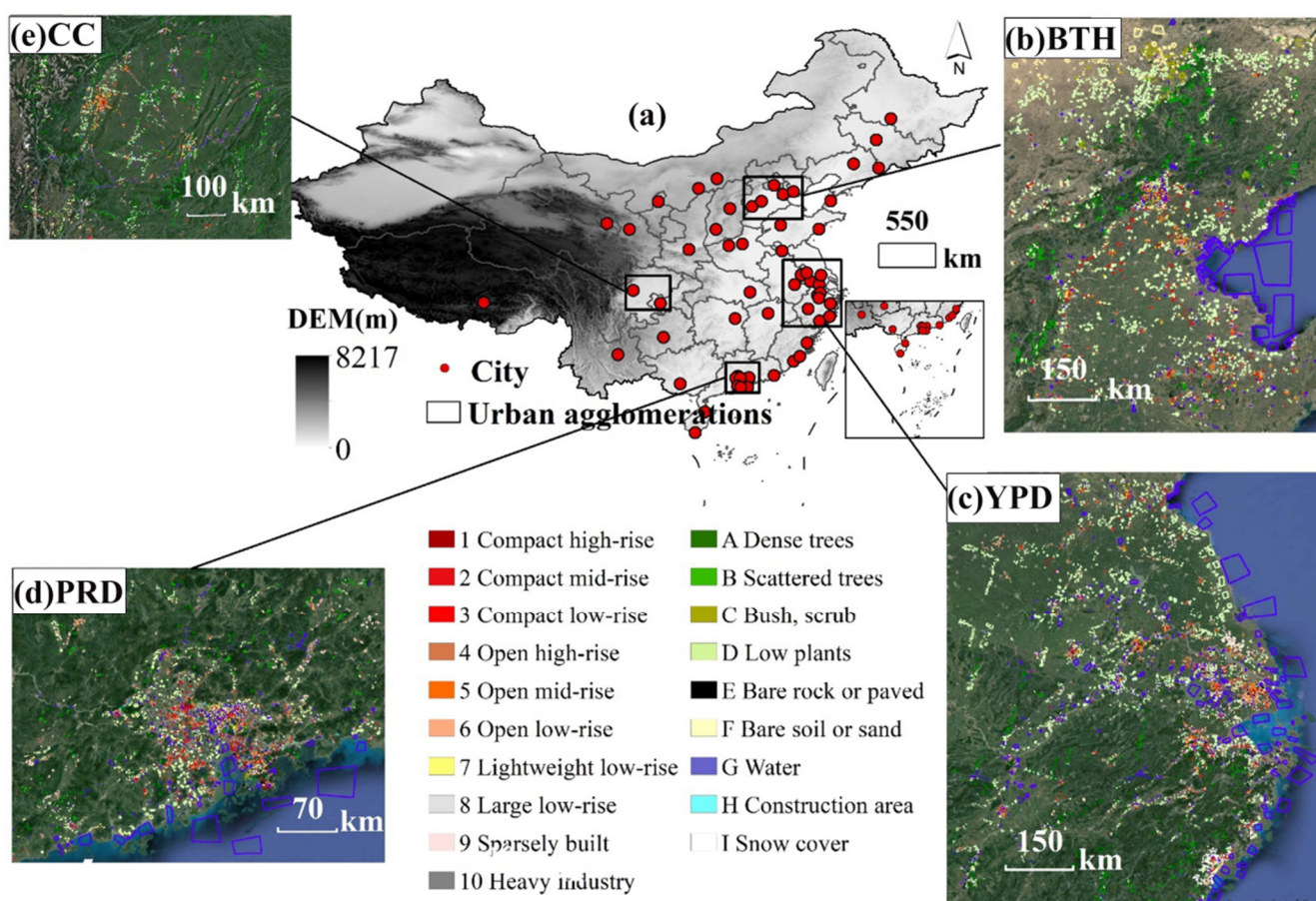
Figure 1. Study area locations (**a**), LCZ classification training samples ((**b**) BTH; (**c**) YPD; (**d**) PRD; (**e**) CC) in selected areas.

2.2. LCZ Classification System and Ground Object Features

The original LCZ classification system defined by Stewart and Oke classifies urban areas into 17 classifications based on land cover, surface structure, building materials and human activities; LCZ 1–10 is the building classification of urban land use, and LCZ A–G is the natural building classification [25]. Based on this, this paper used the WUDAPT method to construct LCZ datasets of 63 cities and 4 urban agglomerations in China. In addition, China is in a stage of rapid urbanization and has a large amount of construction area (Figure 2a). In these areas, the paper added the classification of construction areas, which are land use classifications similar to natural bare or sandy soil, but are construction areas with other building materials. We defined the land use classification of the construction area as an additional LCZ classification (LCZ H). Then, because the plateau northwest of CC is covered with snow throughout the year (Figure 2b), we defined this underlying surface as plateau snow cover (LCZ I).

The characteristics of different buildings and other features in major Chinese cities based on LCZ classification are shown in Table 1. The surface cover characteristics of open high-rise buildings and open mid-rise buildings were similar, with the main difference being building height. The division between open low-rise buildings and sparsely buildings mainly depended on the openness of buildings and the richness of vegetation. Lightweight low-rise buildings, large low-rise buildings, and heavy industries were mostly continuous structures, showing mixed distribution.
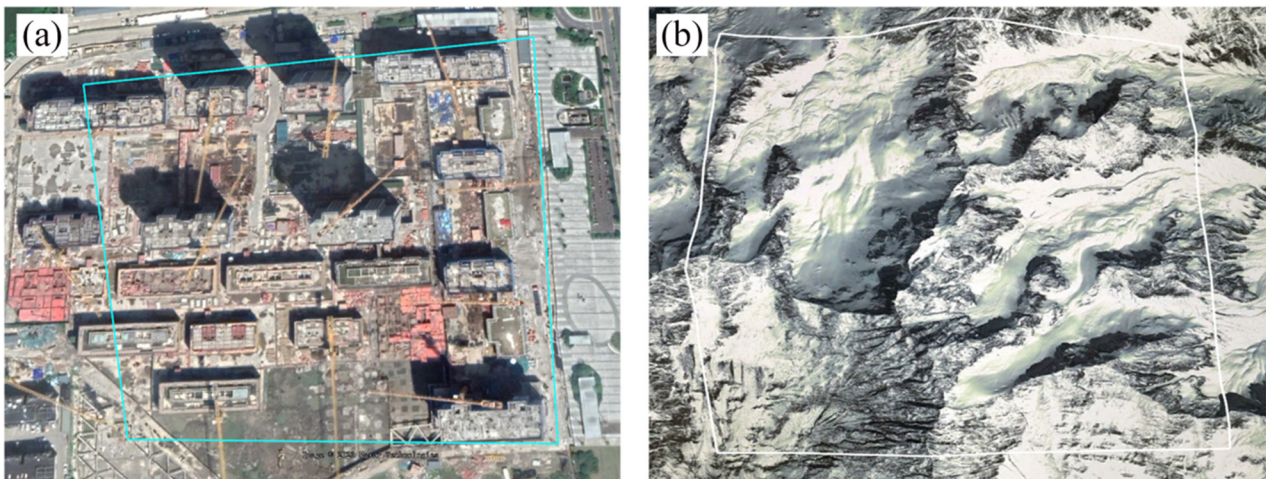
Figure 2. Examples of additional LCZ classifications added in this study: (screenshots from Google Earth): (**a**) construction area (LCZ H) and (**b**) snow cover (LCZ I).

Table 1. Examples of different building classification and other surface features in large Chinese cities (a–s) by LCZ classification (screenshots from Google Earth).
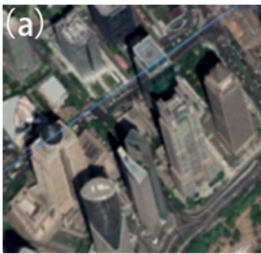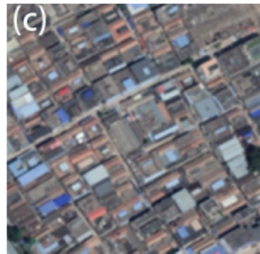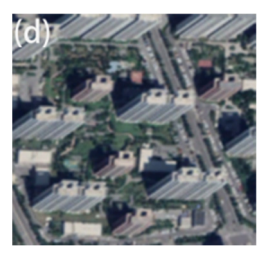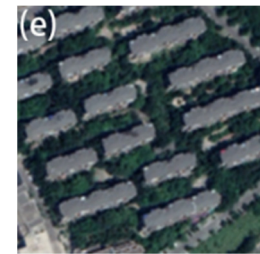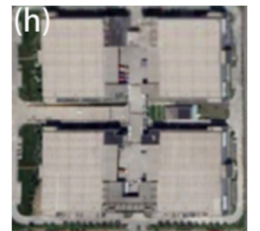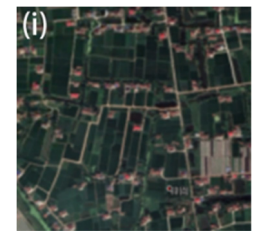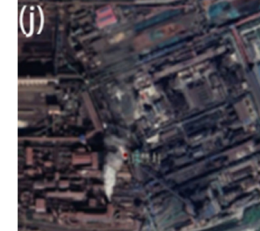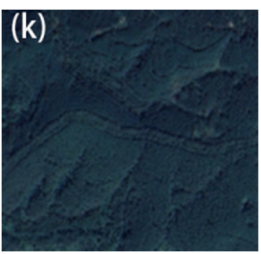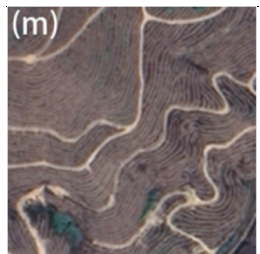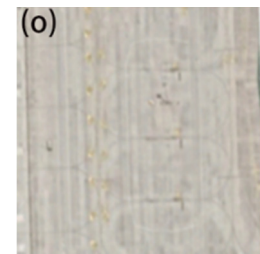
LCZ 1 Compact high-rise	LCZ 2 Compact mid-rise	LCZ 3 Compact low-rise	LCZ 4 Open high-rise	LCZ 5 Open mid-rise
LCZ 6 Open low-rise	LCZ 7 Lightweight low-rise	LCZ 8 Large low-rise	LCZ 9 Sparsely built	LCZ 10 Heavy industry
LCZ A Dense trees	LCZ B Scattered trees	LCZ C Bush, scrub	LCZ D Low plants	LCZ E Bare rock or paved

Table 1. *Cont.*

LCZ F Bare soil or sand	LCZ G Water	LCZ H Construction area	LCZ I Snow cover
(p)	(q)	(r)	(s)

2.3. LCZ Mapping Method

The mapping method was as follows:

(1) Acquisition and preprocessing of Landsat data. We downloaded 246 Landsat 8 images from the USGS Earth-Explorer website (https://earthexplorer.usgs.gov/, accessed on 12 September 2020) for the year 2019. These images comprise 11 multispectral bands and have a cloud cover of less than 3%, with a resolution of 30 m. We performed mosaic, atmospheric correction, splicing, and projection processes on these images, and then resampled them to a resolution of 120 m [28] in order to prepare the data for LCZ classification in SAGA GIS.

(2) In total, 100,000 samples, including ~76,000 training samples and ~23,000 validation samples, were manually created (Figure 1 presents the delineated samples for 4 urban agglomerations, and Figure S1 provides samples for the remaining 63 cities. The small areas enclosed by yellow lines represent the spatial extent of the samples). In this study, Google Earth was used to digitize the Local Climate Zone (LCZ) polygons, which were used as training samples and validation samples for the later generation of LCZ classification [28]. The underlying surface was classified according to the actual topography of the city, and then manually delineated (classification criteria and sampling methods are listed in the World Urban Database web-page: https://www.wudapt.org/digitize-training-areas/, accessed on 16 September 2020); after the completion of each classification, the samples were preserved in the .kmz format. In Google Earth, we digitized the area by manually outlining the points that demarcated the boundaries, and repeated the process several times for each LCZ classification, ensuring that the classification covered all the different looks in the sampled cities. However, to make sure that enough samples were obtained, we spent a lot of time and manpower performing manual sampling; this step is the most important for improving the accuracy of the datasets. Because each city and urban agglomeration had unique characteristics in China, it was difficult for the same training sample set to be applied to more than one location, so we conducted independent sampling for each city and urban agglomeration. Each LCZ class contained 10–100 polygons, except for a few LCZ classifications that had a smaller area. The number of training samples in most LCZ classifications exceeded the number specified in the WUDAPT process. The WUDAPT classification process was initially applied to European cities with regular urban forms (Figure 3a), and 5–15 samples for each LCZ classification were sufficient. However, the morphology of Chinese cities is relatively chaotic (Figure 3b), and the same LCZ classification generally corresponds to a variety of building forms. Therefore, more samples are needed to improve the accuracy of map making. For example, the large low-rise buildings in Figure 3a correspond to different architectural forms, so as many samples as possible should be used for automatic classification.

Figure 3. Examples of different urban forms (screenshot from Google Earth): (**a**) Paris, (**b**) Beijing, and (**c**) large low-rise buildings with different architectural forms.

The sample quality is key to improving the accuracy. When creating samples, the largest homogeneous area in the city should be sought to the greatest extent possible, and the minimum side length of each sample should be greater than 200 m when practical. A buffer of ~100 m was placed between each sample. Overall, we created about 100,000 samples, including 76,000 training samples and 23,000 verification samples.

(3) The LCZ classification was generated by using SAGA GIS software. Landsat 8 remote sensing images including the research area were obtained in Step 1, and the training samples obtained in Step 2 were imported into SAGA GIS for the analytical processing of the remote sensing images [28]. Finally, the random forest classification method in SAGA GIS was used to classify the training samples, and the LCZ map of the selected area was obtained. Then, using comparison with Google Earth high-resolution imagery, the LCZ map was continuously improved by modifying the existing training samples and adding new training samples. This process was repeated until results of satisfactory quality were achieved for LCZ classification.

2.4. Accuracy Assessment

The random point verification method was proposed to evaluate the LCZ datasets with building classification using Google Earth high-resolution images for the same period [53]. A certain proportion of pixels for each LCZ classification was randomly collected on the LCZ map as verification samples, and these were compared with Google Earth images in the same period in order to obtain the accuracy. For cities, the ratio was 0.5% and for urban agglomerations, it was 0.1%. Due to the large urban area, the total number of validation samples used in this paper reached more than 23,000. The evaluation index included the overall accuracy (OA) of all LCZ classifications, the overall accuracy of built classification (OA$_u$), and the overall accuracy of natural land cover classification (OA$_n$), which was defined as follows:

$$OA = \sum_{i=1}^{19} \frac{n_i}{N_i} * p_i \tag{1}$$

$$OA_u = \sum_{i=1}^{10} \frac{n_i}{N_i} * p_i + \frac{n_{18}}{N_{18}} * p_{18} \tag{2}$$

$$OA_n = \sum_{i=11}^{17} \frac{n_i}{N_i} * p_i + \frac{n_{19}}{N_{19}} * p_{19} \tag{3}$$

where i = 1–10, 18 represents the urban land-use classifications LCZ 1–10 and LCZ H; i = 11–17, 19 represents the natural cover classifications LCZ A-G and LCZ I; n represents the correct pixel number at each pixel point of LCZ classification verification; N represents the pixel number of each LCZ classification verification; and p represents the proportion of pixel area corresponding to each LCZ classification in the pixel area corresponding to all LCZ classifications in each city or agglomeration. Equation (2) represents the proportion of LCZ corresponding to urban land use classifications for all urban land use classifications and

Equation (3) represents the proportion of LCZ corresponding to natural cover classifications in all natural cover classifications.

3. Results and Discussion

3.1. LCZ Map

The resulting LCZ maps of the 4 urban agglomerations and 63 cities are shown in Figures 4 and 5, which clearly show the spatial structures and detailed building distribution characteristics. Differences in geographical climate, cultural habits, and economic development levels in different regions have led to obvious differences in urban forms. In China, the spatial layout of most cities is blocky, such as in Beijing and Chengdu. Some cities, such as Lanzhou and Lhasa, are distributed along river valleys, rivers or coastlines in strips. Other cities, such as Chongqing and Wuhan, are distributed in clusters due to the limitations of physical and geographical conditions. A few cities are annular (Xiamen) or star-shaped (Guangzhou). Generally speaking, the shape of Chinese big cities is more complex. Among the four major urban agglomerations, the urbanization level of the Pearl River Delta is higher, the construction area is constantly expanding, the gap between cities is small, and it is gradually developing into agglomerations.
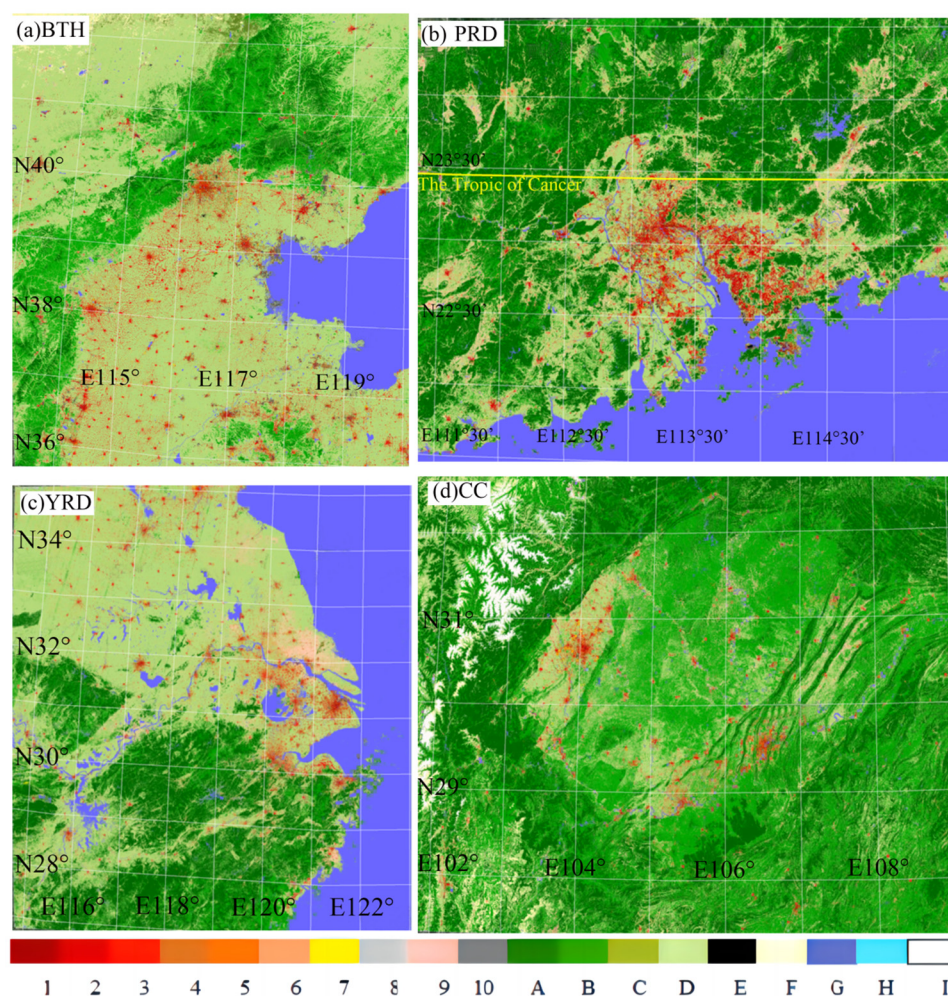

Figure 4. LCZ classification results for the four urban agglomerations. based on WUDAPT (LCZ 1-I classifications are shown in Table 1).
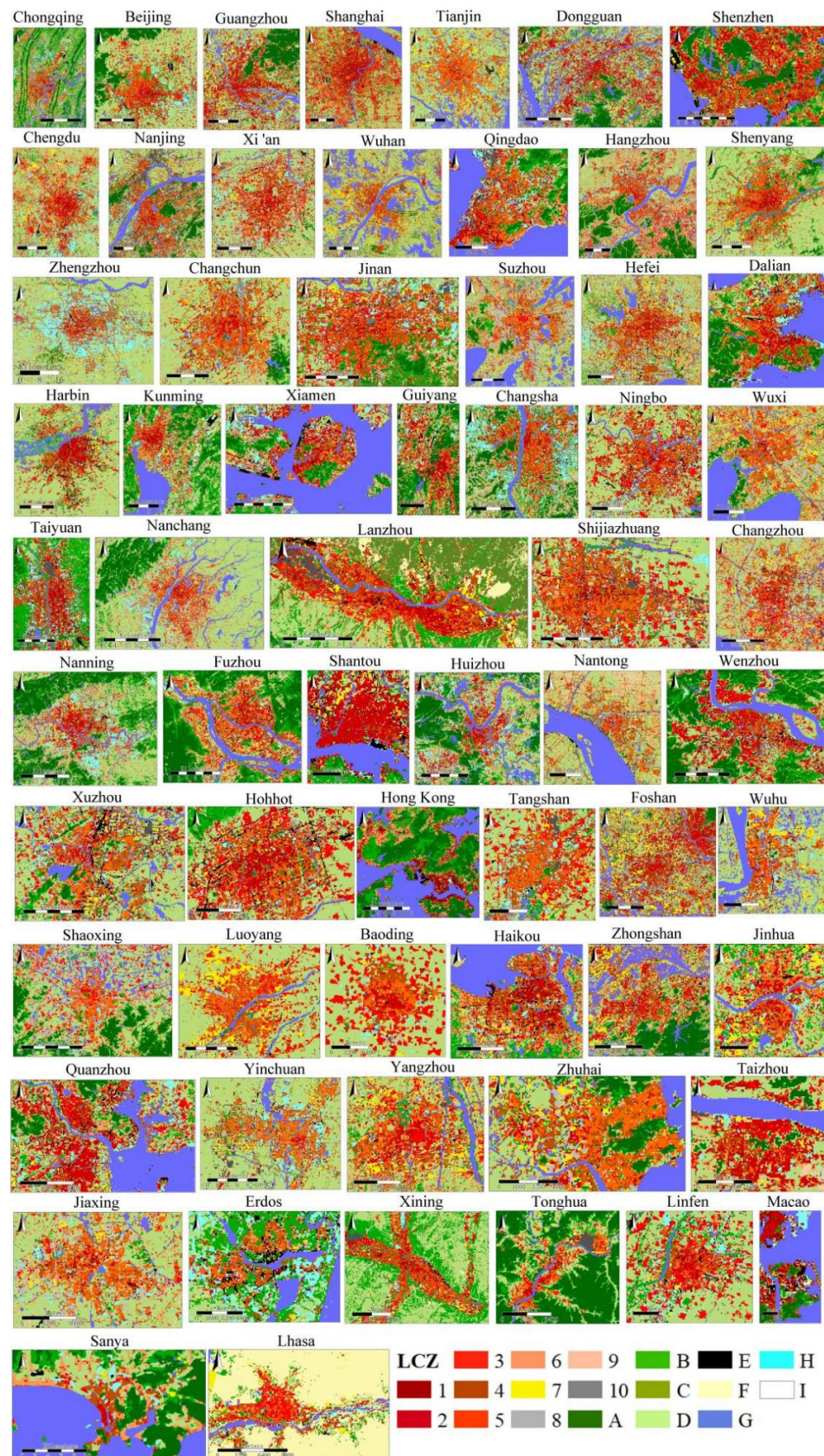
Figure 5. LCZ classification results for the 63 cities based on WUDAPT (LCZ 1-I classifications are shown in Table 1).

3.2. Overall Accuracy

We evaluated the datasets using validation samples independent of the training set. The LCZ datasets were generally of good quality. Figure 6 shows the LCZ classification accuracy of the 63 cities and 4 urban agglomerations, and the sample number of each city. The OA range for all cities was 71–93% (mean 82%). The OAn was greater than 80%, while the OA_u range was 57–83% (mean 72%). Nanjing, Guiyang, Lhasa had an OA_u of slightly less than 60%, Chongqing and Wuxi had an OA_u of slightly more than 80%, and the rest of the cities had an OA_u between 60 and 80%. This is higher than the results of similar domestic studies (Table 2). In this paper, the training samples of each city or region are nearly saturated (Figure 6). This shows that the use of high-quality and sufficient samples is the key to obtaining high accuracy.
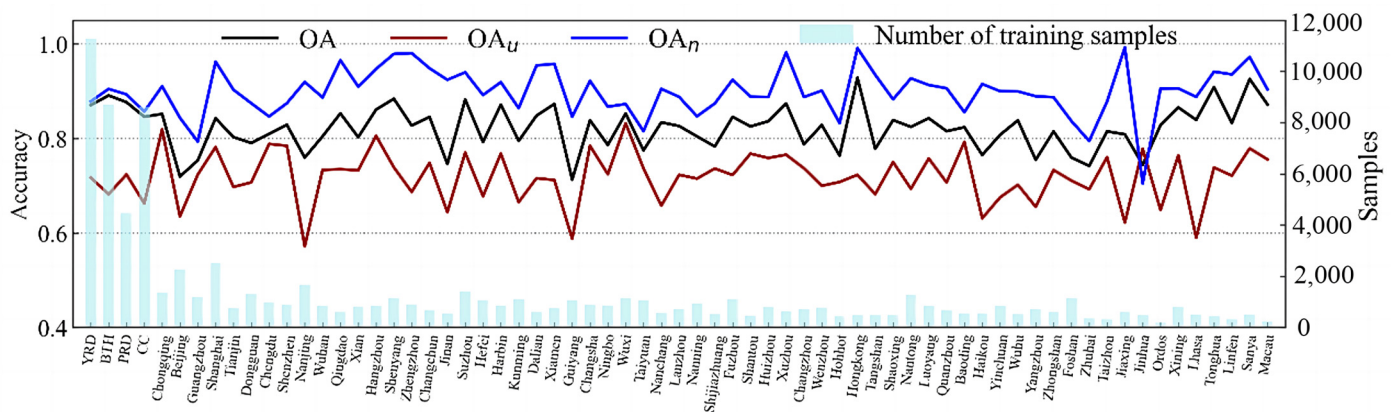

Figure 6. Overall accuracy of LCZ maps and number of training samples by city and region.

Table 2 shows data precision comparison of the data regarding the existing LCZ classification work based on the WUDAPT method. It can be seen that the OA_u of LCZ data for most other countries ranges between 54 and 96%, which is larger than that of the Chinese cities. Among the Chinese cities, only Shi et al. [58]. could reach an OA_u of 84% in the study of Guangzhou, while the rest were basically below 61% and the lowest was only 26%. Compared to the existing Chinese city studies, the OA_u of our data has improved, and ranges between 66 and 72%. Urban agglomerations such as BTH, YRD and PRD have always been the hot areas of land use classification research in China. Compared with the results of similar domestic studies, our OA values were 23%, 20%, and 12% higher for BTH, YRD, and PRD, respectively (Table 2). We attributed this to the number of training samples (76,000, much higher than in other studies, as shown in Table 2), the strict evaluation of sample quality through visual interpretation during the labeling process, and the uniformity and appropriate size of the training sample sets. China's unique and complex urban form has high requirements for sample size and quality, and the large cities need a sufficient number of training samples and a good sample quality in order to obtain LCZ maps with high accuracy.

Compared with European and American cities [59] (Table 2), the overall accuracy of Chinese cities is low. This is because the urban population and economic development level of different regions differ greatly, resulting in different urban structures and forms [60–65], leading to differences in accuracy. China has been urbanizing rapidly for more than 20 years, with the rapid and drastic evolution of urban form and the unprecedented expansion of urban space; this presents urban characteristics that are completely different from those of European and American cities. European and American cities have formed a regular and stable morphological texture under refined planning and control, while Chinese cities have a relatively chaotic morphological texture under extensive planning and management. Therefore, the LCZ identification of urban underlying surfaces in China is also relatively chaotic, resulting in a low accuracy.

Table 2. Comparison of WUDAPT-based LCZ mapping results by region.

Area	Reference	City	Data Source	The Number of Training Samples	$\overline{OA}$
Europe and the United States	Bechtel et al. [28]	Houston	Landsat, Google Earth	128	96%
	Wang et al. [41]	Phoenix	Landsat, Google Earth	——	82%
		Las Vegas	Landsat, Google Earth	——	82%
	Demuzere et al. [43]	All cities in Europe	Sentinel-1 SAR, Various spectral data	2700	>95%
	Fonte et al. [44]	Hamburg	Landsat, OSM, Google Earth	——	58%
	Verdonck et al. [48]	Antwerp	Landsat, Google Earth	79	86%
		Brussels		74	80%
		Ghent		100	90%
	McRae et al. [53]	San Jose	Landsat, Google Earth	921	62%
	Mouzourides et al. [59]	London	Landsat, Google Earth	312	75%
India	Patel et al. [14]	Mumbai	Landsat, Google Earth	——	86%
Sudan	Bechtel et al. [28]	Khartoum	Landsat, Google Earth	——	97%
Zimbabwe	Mushore et al. [54]	Harare	Landsat, Google Earth	157	96%
Thailand	Khamchiangta et al. [60]	Bangkok	Landsat, Google Earth	——	76%
Japan	Zhou et al. [65]	Sendai	Landsat, Google Earth	——	93%
China	Wang et al. [41]	Hong Kong	Landsat, Google Earth	850	76%
	Ren et al. [45]	20 cities in China	Landsat, Google Earth	850	75%
	Cai et al. [55]	Guangzhou	Landsat, Google Earth	850	84%
	Cai et al. [56]	YRD Shanghai Hangzhou	Landsat, Google Earth, Aster	850	67%
	Shi et al. [58]	BTH	Landsat, Google Earth	——	58%
	Wang et al. [57]	YRD	Landsat, Google Earth	——	76%
	Xu et al. [61]	Guangzhou	Landsat, Google Earth	29,725	62%
	Matthias Demuzere et al. [62]	PRD	Landsat8, PALSAR, Sentinel-1, Sentinel-2, VIIRS	400	75%
	This study	Guangzhou	*Landsat, Google Earth*	1800	67%
				2100	76%
				——	80%
		PRD		1700	76%
		Beijing		——	72%
		Harbin		——	72%
		Lhasa		——	70%
		63 major cities and 4 regions in China		*76,000*	*82%*
		BTH		*9100*	*89%*

Figure 6 also shows the sample number of each city. Since the size of the urban area and the area of the samples are different, the number of samples is not well correlated with accuracy. However, in the process of data processing, we did significantly improve the accuracy of the data by adding more samples. When the number of training samples is saturated, the accuracy depends on the complexity of the urban form. In cities with orderly urban planning, such as Shanghai, Suzhou and Wuxi, the LCZ identification results have a high accuracy. However, in cities with complex urban forms, such as Beijing, Guangzhou, Guiyang and Nanjing, buildings of different heights are highly mixed and spectral information recognition is confused, resulting in a relatively low accuracy.

This study established datasets of 100,000 samples, including approximately 76,000 training samples and 23,000 validation samples. After the creation of samples, the samples in this study can be utilized for further research addressing the establishment of urban land use datasets in China. Additionally, with the advancement of machine learning techniques, we can employ more advanced machine learning methods to generate Chinese LCZ datasets [63–65]. In addition, the datasets established in this study can also provide some auxiliary information for other studies, such as SWAP mission retrieval algorithms [66].

3.3. Accuracy Evaluation of Typical Large Cities and Urban Agglomerations

Due to inconsistencies in the economic development levels, regional planning, local policies, and climatic conditions among different regions, the patterns and architectural forms of cities and urban agglomerations differ widely, which in turn leads to differences in LCZ classification accuracies. To compare the accuracy of the LCZ classification results in different regions and the adaptability of the WUDAPT method in the transition from cities to urban agglomerations, we focused further on the four urban agglomerations and typical large cities within them (Beijing, Shanghai, Guangzhou, and Chengdu).

3.3.1. Overall Accuracy of Four Urban Agglomerations

In the process of LCZ classification, we found that the OA and OA_n values of the four major urban agglomerations were both >85%, but the OA_u was lower, with CC as low as 66% (Table 3). This is mainly due to the large proportion of vegetation classifications in this urban agglomeration. The spectral information of vegetation classifications is easy to classify, and the accuracy of OA_n is high, which leads to the high accuracy of OA. From the results in Figure 7 and Table 2, it can be seen that the urban classification accuracy of a single city is higher than that of urban agglomerations in most cases. For OA_u, Shanghai and Chengdu were higher than YRD and CC, and Guangzhou was similar to PRD (Table 3).

Table 3. Accuracy difference of LCZ classification results between urban agglomeration and typical large cities within those agglomerations.

Urban Agglomeration or City	OA (%)	OA_u (%)	OA_n (%)
YRD	87	72	88
Shanghai	84	78	96
BTH	89	68	90
Beijing	72	64	84
PRD	88	72	89
Guangzhou	75	72	79
CC	85	66	86
Chengdu	81	79	85

The overall accuracy and the accuracy of the urban land classification in Shanghai were the highest. Combined with a Google online map (www.google.com.hk/maps/, accessed on 20 September 2020), the urban form of Shanghai is generally regular, so the recognition of LCZ is relatively accurate, with the highest overall accuracy of 83%. Because of its history and society, and because Beijing is the core region of traditional architecture and modern building, mutual crisscross, collocation and a mixed peripheral core area owing to urbanization have led to landscape fragmentation (Figure 3b) and the formation of a complex texture pattern. Its highly heterogeneous urban form makes the overall accuracy of the built classifications (OAu) of Beijing low, at only 64%.
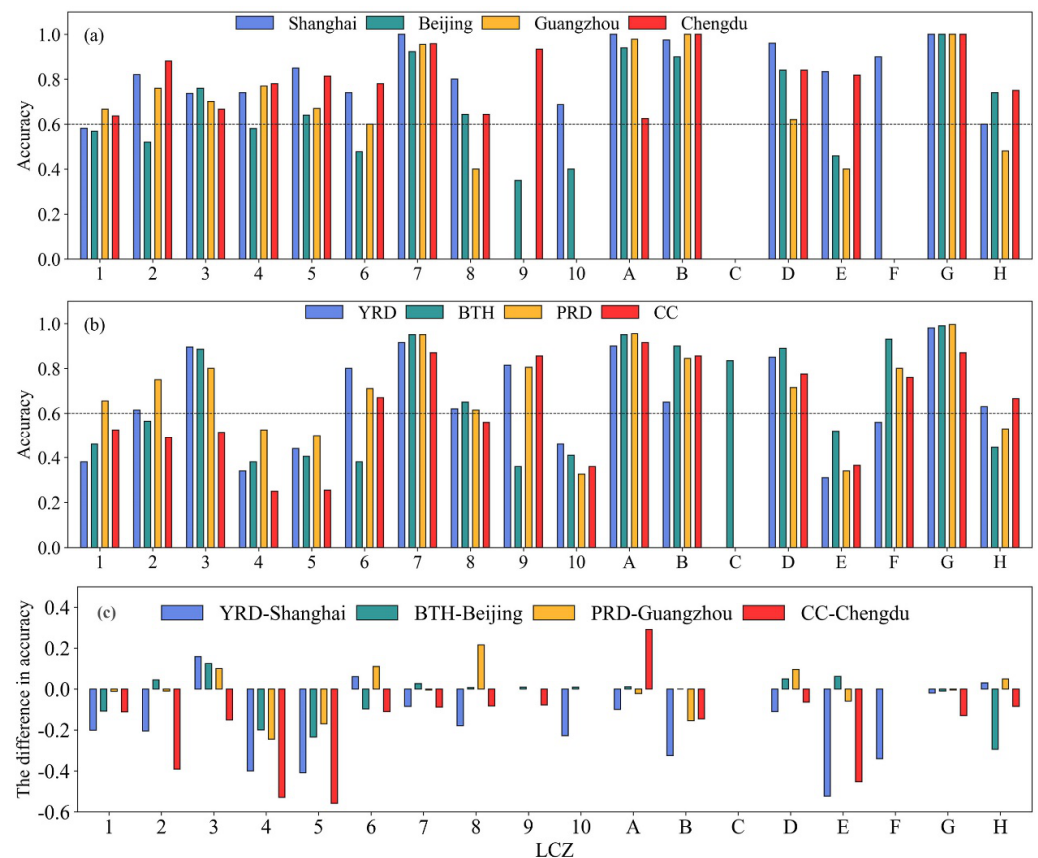
Figure 7. LCZ classification accuracy differences between large cities and the urban agglomerations containing them. (**a**) the accuracy of each LCZ classification in the four cities of Shanghai, Beijing, Guangzhou and Chengdu; (**b**) the accuracy of each LCZ classification of YRD, BTH, PRD and CC urban agglomerations; (**c**) LCZ classification accuracy differences between large cities and the urban agglomerations).

3.3.2. Classification Accuracy Per Class

The classification performance of most urban classifications (LCZ 1–10) in cities was better than that in urban agglomerations, and the accuracy was about 60% or higher, with lightweight low-rise buildings (LCZ 7) being highest at >90% (Figure 7). The classification results for most built classifications in Beijing were poor, with the accuracies of compact mid-rise buildings (LCZ 2), open low-rise buildings (LCZ 6), sparsely built (LCZ 9), and heavy industry (LCZ 10) all being <60%. Among the natural cover classifications, the accuracy of dense trees (LCZ A), scattered trees (LCZ B), and water (LCZ G) in all major cities was higher, especially the latter (100%). The proportion of bare rock or paved (LCZ E) in large cities was relatively small, and there were fewer samples available for training, leading to an unstable classification performance.

The LCZ classification accuracy in urban agglomerations varied greatly. Compact mid-rise buildings (LCZ 2), lightweight low-rise buildings (LCZ 7), and sparsely built buildings (LCZ 9) performed better than other built classifications, but open high-rise building (LCZ 4), open mid-rise building (LCZ 5), heavy industry (LCZ 10), and bare rock or paved (LCZ E) were poor (<60%). Comparing the classification results of cities and urban agglomerations, the accuracy rate of open mid-rise and high-rise buildings was significantly reduced. Therefore, the LCZ classification of large-scale urban agglomerations based on WUDAPT still has limitations in terms of the accuracy of partial LCZ classification.

3.3.3. Reasons for the Difference in LCZ Classification Accuracy

Due to complex Chinese urban morphology, the accuracy of some LCZ classifications remains low because of their high mixing in the underlying surface. Confusion matrices (Figure 8) showed that some large low-rise buildings (LCZ 8), compact mid-rise buildings (LCZ 2), and compact low-rise buildings (LCZ 3) in YRD were classified as LCZ 1, leading to a low accuracy for that class. Similar confusion occurred in BTH and CC. There are no data for building height characteristics in the WUDAPT method, and it is difficult to effectively identify the classification of different building heights, which is one of the reasons for the reduced accuracy. Furthermore, compact high-rise buildings were often mixed with large low-rise buildings and compact mid-rise buildings, resulting in confusion (Figure 9a,b). In addition, lightweight low-rise buildings (LCZ 7), large low-rise buildings (LCZ 8), and heavy industry buildings (LCZ 10) in the large urban agglomerations were often confused because of their mixed distribution (Figure 9c). This occurred because Chinese cities and urban agglomerations tend to have more small factories, which are classified as lightweight low-rise buildings (LCZ 7) or large low-rise buildings (LCZ 8), and many with heavy industry have a mixed distribution of water towers, storage tanks, and other vertical features, leading to confusion. A similar pattern was discussed by Liu et al. [67].
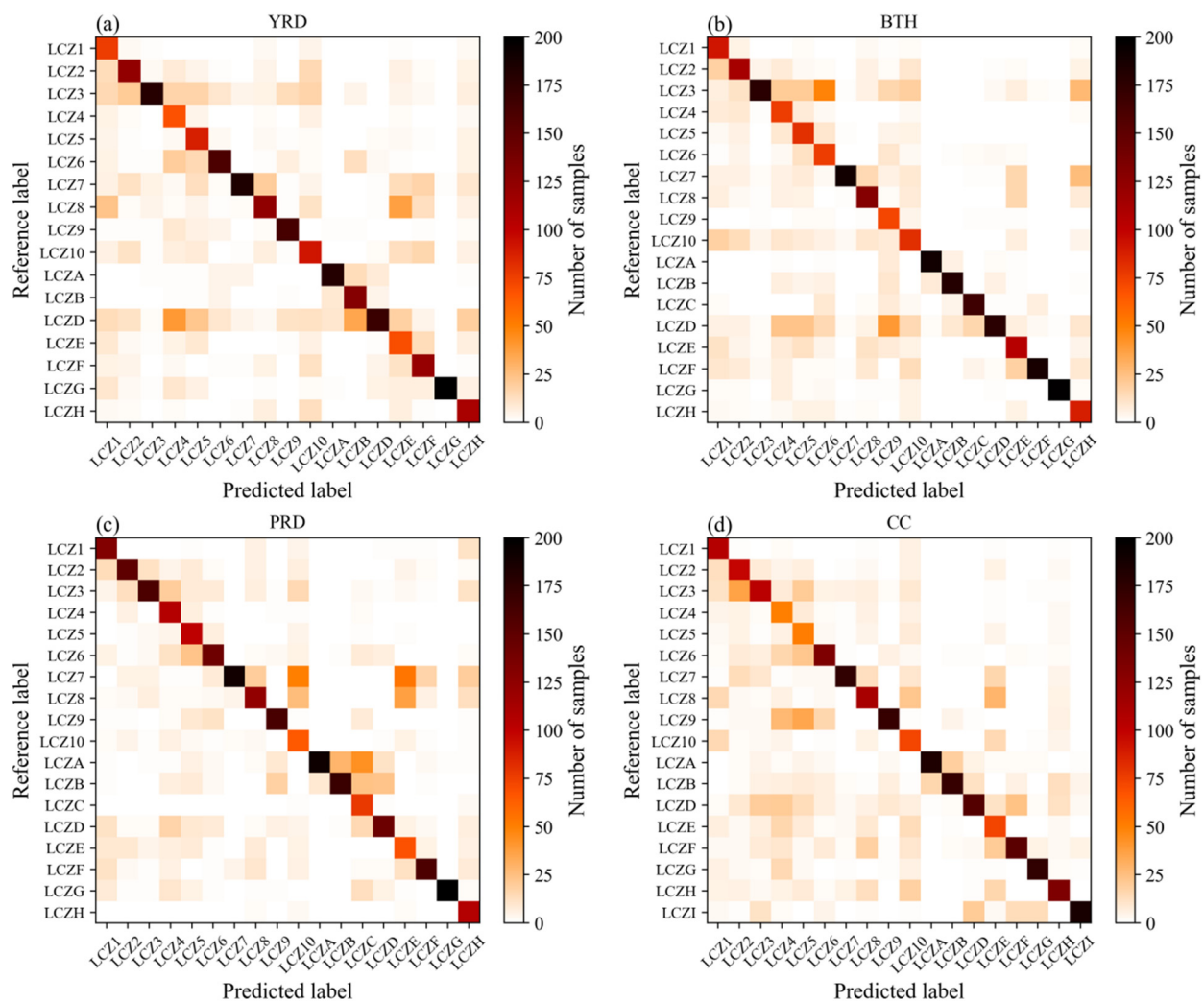

Figure 8. Confusion matrices for the four major urban agglomerations (LCZ1~H are LCZ classifications, as shown in Table 1).

Figure 9. Examples of mixed industrial classifications (screenshots from Google Earth).

In addition, some LCZ classifications were confused because of surface similarities. For example, large low-rise buildings (LCZ 8) were wrongly classified as bare rock or paved (LCZ E) in all four urban agglomerations because the optical properties of the two were similar (Figure 10a,b) and the only difference was building height; indeed, building height is difficult to distinguish using existing methods. Similar confusion occurred between open mid-rise buildings (LCZ 5) and open low-rise buildings (LCZ 6) (Figure 10c,d), as well as between dense trees (LCZ A) and scattered trees (LCZ B), which was also observed by Demuzere et al. [43]. Therefore, in future LCZ mapping, auxiliary datasets with building height and vegetation information should be added as input features to the traditional two-dimensional remote sensing images, in order to obtain a better classification map.

Figure 10. Examples of similar LCZ classifications causing confusion (screenshots from Google Earth. LCZ 8: large low-rise buildings, LCZ E: bare rock or paved, LCZ 5: open mid-rise buildings, LCZ 6: open low-rise buildings).

When the WUDAPT method was applied to the LCZ classification of a large area in China, the classification effect for a mixed distribution of buildings and vegetation was significantly worse, especially for open mid-rise and high-rise buildings (LCZ 4 and LCZ 5) (Figure 8), which is consistent with Yoo et al. [63]. According to the confusion matrices, these two LCZ classifications were not only confused with LCZ classifications

with similar morphology (such as LCZ 6), but also with low plants (LCZ D), so the resulting accuracy was low. This indicated that LCZ classification based on the similarity of spectral information is desirable for most LCZ classifications, but that for a mixed distribution of buildings and vegetation, it was not ideal.

In addition, some LCZ classifications covered relatively small areas, leading to an imbalance in the LCZ training samples. For example, hardened ground in the four urban agglomerations, bush and shrub (LCZ C) in PRD, and open low-rise buildings (LCZ 6) and sparsely built (LCZ 9) in BTH accounted for a relatively small amount of the underlying surface, leading to a small number of training samples that could provide moderate size and uniform coverage, and thus an imbalance in the training samples. Solving this issue will be an important direction for future research.

The main factors affecting the differences in the LCZ classification accuracy included the high mixing score of some LCZ classifications in the underlying surface, the similarity between LCZ classifications (lack of building height information), and the lack of high-quality training samples due to their small size. Further research should add additional auxiliary datasets, such as Sentinel-2 multispectral instrument (MSI), Sentinel-1 synthetic aperture radar (SAR), Luojia1-01 nighttime light (NTL), and Open Street Map (OSM) datasets, as input features to improve the classification effect and resolution of the datasets [49,50].

3.4. Proportion of LCZ Classifications Newly Added in Big Cities

Based on the actual underlying surface conditions in China, we added construction area (LCZ H) and snow cover (LCZ I) to the original LCZ classifications and assessed their proportions on the underlying surface (Figure 11). LCZ H was widely distributed in large cities, with 35% of urban construction areas accounting for more than 5% of the entire underlying surface (Figure 11a). The proportion of construction areas in urban land use classifications was even higher, with 70% of construction areas accounting for >5% (Figure 11b). These cities were mostly large cities (sub-provincial cities and municipalities directly under the central government), consistent with Liu et al. [67]. In addition, urban expansion in China was concentrated not only in North and Central China, but also in Southwest China. For example, in Chongqing, Chengdu, Kunming, and Guiyang, construction area accounted for 7.91%, 8.45%, 6.17%, and 6.43% of the study area, respectively. Perennial snow cover in the northwestern CC (LCZ I) accounted for 2%.
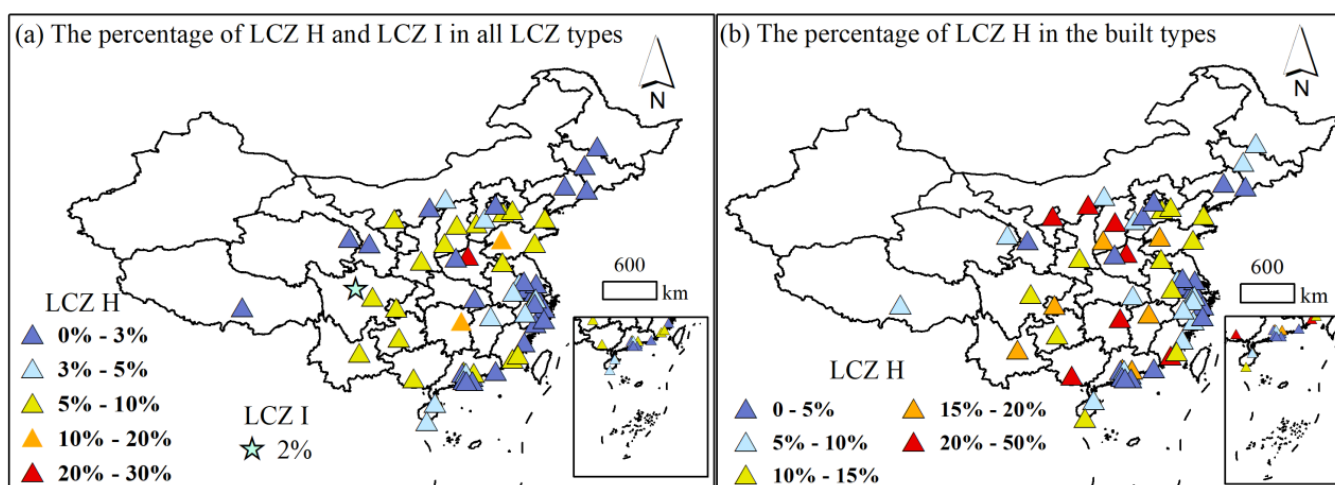

Figure 11. (**a**) Proportion of LCZ H and LCZ I in all LCZ classifications and (**b**) proportion of LCZ H in all urban land use classifications.

Construction area mainly occupied agricultural land and low-rise buildings in rural areas, and its proportion can represent the extent of urban expansion to some extent. For

example, in coastal Beijing and inland Chengdu, 8.4% and 9.7% of land use were identified as construction area (LCZ H), respectively. The LCZ maps of Beijing (Figure 12a) and Chengdu (Figure 12b) showed that the construction areas of the two cities were mostly located at the intersections between urban and rural areas or suburbs. Further assessment using Google Earth screenshots demonstrated that the surface of the construction areas was complex, usually a mixture of soil and building materials, with properties similar to bare soil or sand (LCZ F).
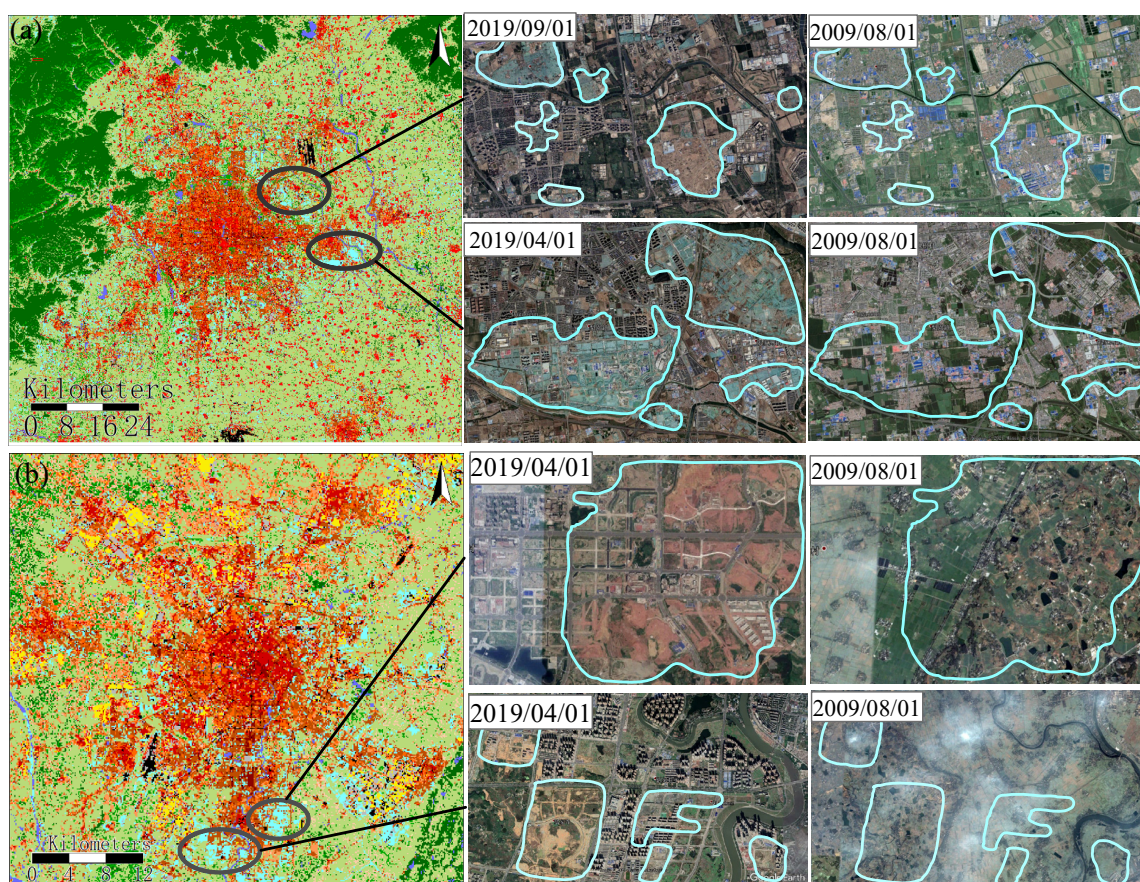

Figure 12. Distribution of construction area and changes in underlying surface over time in (**a**) Beijing and (**b**) Chengdu (the representative construction area framed by the blue line).

For Beijing, construction areas mainly replaced buildings in suburban areas, which were mainly composed of compact low-rise buildings (LCZ3), low plants (LCZD), and small factories (Figure 12a), thus becoming an important LCZ classification in Beijing. In contrast, construction areas in Chengdu mainly replaced low plants (LCZ D), open low-rise buildings (LCZ 6), and sparsely built (LCZ 9) in suburban and rural areas (Figure 12b). In 2009, low-and low-rise buildings dominated the suburban areas of Chengdu, while by 2019, the underlying surfaces and small areas of open low-rise buildings dominated by low plants were replaced by construction areas, whose proportion in suburban areas increased significantly.

4. Conclusions

We used multi-temporal Landsat 8 satellite data from 2019 to construct WUDAPT-based LCZ datasets for 63 cities and 4 urban agglomerations in China. The OA of these datasets was 71–93% (mean 82%), that of urban classifications was 57–83% (mean 72%), and that of natural classifications was 70–99% (mean 90%). The classification results showed good performance overall and can be used in fine weather forecasting, atmospheric environment simulation forecasters, climate change assessment, and urban planning.

In this study, nearly 76,000 samples were obtained for LCZ classification, and another 23,000 samples were used to evaluate the data accuracy, with a total of nearly 100,000 samples. The sample data are expected to serve well in the creation of LCZ maps of larger regions in the future.

Chinese urban construction areas account for a large proportion of land use. However, the original definition of LCZ by Stewart and Oke (2012) contained no such classification. Therefore, this underlying surface classification was defined as LCZ H in this study. Similarly, the plateau in the northwestern CC is covered with snow throughout the year, so this underlying surface classification was defined as LCZ I in this study.

5. Limitations and Outlook

There were some limitations to creating the WUDAPT-based LCZ datasets. First, Landsat 8 data were used in this study. In the creation of future datasets, the use of higher resolution satellite data, such as Sentinel, will have a positive impact on the resolution and accuracy of the data. The main factors affecting the differences in LCZ classification accuracy included the high mixing score of some LCZ classifications in the underlying surface, the similarity between LCZ classifications (lack of building height information), and the lack of high-quality training samples due to their small size. Further research should add additional auxiliary datasets, such as Sentinel-2 multispectral instrument (MSI), Sentinel-1 synthetic aperture radar (SAR), Luojia1-01 nighttime light (NTL), and Open Street Map (OSM) datasets, as input features to improve the classification effect and resolution of the datasets. Second, the verification data were only derived from Google Earth, while more objective and authoritative data, such as urban building data, were not adopted for verification, making the accuracy of the data dependent upon the previous experience and geographical knowledge of the data verifier to a greater extent. Third, a large number of training samples were artificially collected. Although this guaranteed the accuracy of the LCZ datasets, it required extensive human and material resources. Future work should test the use of an advanced machine learning algorithm to create such maps. Furthermore, although the datasets in this paper were drawn from 2019 conditions, the rapid Chinese urbanization process and the ongoing drastic changes in the underlying surface mean that these datasets needs to be updated regularly. In addition, the samples in this study can provide references for the establishment of urban land-use datasets. Meanwhile, the LCZ datasets used in this study are not limited to China, but also have the potential to be widely used, and could help to improve the retrieval algorithms of other satellite products. Further, their application in urban weather and climate prediction, as well as in air pollution propagation models, needs further research.

References

1. Li, J.; Mahalov, A.; Hyde, P. Simulating the effects of chronic ozone exposure on hydrometeorology and crop productivity using a fully coupled crop, meteorology and air quality modeling system. *Agric. For. Meteorol.* **2018**, *260–261*, 287–299. [CrossRef]
2. Jee, J.-B.; Kim, S. Sensitivity Study on High-Resolution Numerical Modeling of Static Topographic Data. *Atmosphere* **2016**, *7*, 86. [CrossRef]
3. Su, X.; Wang, F.; Zhou, D.; Zhang, H. Assessing the Spatial Variability of Daytime/Nighttime Extreme Heat Waves in Beijing under Different Land-Use during 2011–2020. *Land* **2022**, *11*, 1786. [CrossRef]
4. Macinnis-Ng, C.M.; Flores, E.E.; Müller, H.; Schwendenmann, L. Throughfall and stemflow vary seasonally in different land-use type in a lower montane tropical region of Panama. *Hydrol. Process.* **2014**, *28*, 2174–2184. [CrossRef]
5. Li, Y.; Liu, D.; Li, T.; Fu, Q.; Liu, D.; Hou, R.; Meng, F.; Li, M.; Li, Q. Responses of spring soil moisture of different land use type to snow cover in Northeast China under climate change background. *J. Hydrol.* **2022**, *608*, 127610. [CrossRef]
6. Deng, J.; Xiao, J.; Ouimette, A.; Zhang, Y.; Sanders-DeMott, R.; Frolking, S.; Li, C. Improving a Biogeochemical Model to Simulate Surface Energy, Greenhouse Gas Fluxes, and Radiative Forcing for Different Land Use type in Northeastern United States. *Glob. Biogeochem. Cycles* **2020**, *34*. [CrossRef]
7. Mohan, M.; Kandya, A. Impact of urbanization and land-use/land-cover change on diurnal temperature range: A case study of tropical urban airshed of India using remote sensing data. *Sci. Total Environ.* **2015**, *506–507*, 453–465. [CrossRef]
8. Chenchao, Z.; Min, X. Land use and anthropogenic heat modulate ozone by meteorology: A perspective from the Yangtze River Delta region. *Atmos. Chem. Phys.* **2022**, *22*, 1351–1371.
9. Thunis, P.; Rouil, L.; Cuvelier, C.; Stern, R.; Kerschbaumer, A.; Bessagnet, B.; Schaap, M.; Builtjes, P.; Tarrason, L.; Bedogni, M.; et al. Analysis of model responses to emission-reduction scenarios within the CityDelta project. *Atmos. Environ.* **2006**, *41*, 208–220. [CrossRef]
10. Ribeiro, I.; Martilli, A.; Falls, M.; Zonato, A.; Villalba, G. Highly resolved WRF-BEP/BEM simulations over Barcelona urban area with LCZ. *Atmos. Res.* **2021**, *248*, 105220. [CrossRef]
11. Zonato, A.; Martilli, A.; Di Sabatino, S.; Zardi, D.; Giovannini, L. Evaluating the performance of a novel WUDAPT averaging technique to define urban morphology with mesoscale models. *Urban Clim.* **2020**, *31*, 100584. [CrossRef]
12. Franco, D.M.P.; de Fatima Andrade, M.; Ynoue, R.Y.; Ching, J. Effect of Local Climate Zone (LCZ) classification on ozone chemical transport model simulations in Sao Paulo, Brazil. *Urban Clim.* **2019**, *27*, 293–313. [CrossRef]
13. Yang, H.; Leng, Q.; Xiao, Y.; Chen, W. Investigating the impact of urban landscape composition and configuration on PM2.5 concentration under the LCZ scheme: A case study in Nanchang, China. *Sustain. Cities Soc.* **2022**, *84*, 104006. [CrossRef]
14. Patel, P.; Karmakar, S.; Ghosh, S.; Niyogi, D. Improved simulation of very heavy rainfall events by incorporating WUDAPT urban land use/land cover in WRF. *Urban Clim.* **2020**, *32*, 100616. [CrossRef]
15. Zhang, Y.; Cao, S.; Zhao, L.; Cao, J. A case application of WRF-UCM models to the simulation of urban wind speed profiles in a typhoon. *J. Wind. Eng. Ind. Aerodyn.* **2022**, *220*, 104874. [CrossRef]
16. Patel, P.; Jamshidi, S.; Nadimpalli, R.; Aliaga, D.G.; Mills, G.; Chen, F.; Demuzere, M.; Niyogi, D. Modeling Large-Scale Heatwave by Incorporating Enhanced Urban Representation. *J. Geophys. Res. Atmos.* **2022**, *127*. [CrossRef]
17. Mughal, M.O.; Li, X.X.; Norford, L.K. Urban heat island mitigation in Singapore: Evaluation using WRF/multilayer urban canopy model and local climate zones. *Urban Clim.* **2020**, *34*, 100714. [CrossRef]
18. Zhang, Z.; Wang, X.; Zhao, X.; Liu, B.; Yi, L.; Zuo, L.; Wen, Q.; Liu, F.; Xu, J.; Hu, S. A 2010 update of National Land Use/Cover Database of China at 1:100000 scale using medium spatial resolution satellite images. *Remote Sens. Environ.* **2014**, *149*, 142–154. [CrossRef]
19. Gong, P.; Liu, H.; Zhang, M.; Li, C.; Wang, J.; Huang, H.; Clinton, N.; Ji, L.; Li, W.; Bai, Y.; et al. Stable classification with limited sample: Transferring a 30-m resolution sample set collected in 2015 to mapping 10-m resolution global land cover in 2017. *Sci. Bull.* **2019**, *64*, 370–373. [CrossRef]
20. Shahzad, M.; Zhu, X.X. Automatic detection and reconstruction of 2-D/3-D building shapes from spaceborne TomoSAR point clouds. *IEEE Trans. Geosci. Remote Sens.* **2015**, *54*, 1292–1310. [CrossRef]
21. Zheng, Y.; Weng, Q. Model-driven reconstruction of 3-D buildings using LiDAR data. *IEEE Geosci. Remote Sens. Lett.* **2015**, *12*, 1541–1545. [CrossRef]
22. Wang, P.; Huang, C.; Tilton, J.C. Mapping Three-dimensional Urban Structure by Fusing Landsat and Global Elevation Data. *arXiv* **2018**, arXiv:1807.04368.
23. Awrangjeb, M.; Gilani, S.A.N.; Siddiqui, F.U. An Effective Data-Driven Method for 3-D Building Roof Reconstruction and Robust Change Detection. *Remote. Sens.* **2018**, *10*, 1512. [CrossRef]
24. Ching, J.; Mills, G.; Bechtel, B.; See, L.; Feddema, J.; Wang, X.; Ren, C.; Brousse, O.; Martilli, A.; Neophytou, M.; et al. WUDAPT: An Urban Weather, Climate, and Environmental Modeling Infrastructure for the Anthropocene. *Bull. Am. Meteorol. Soc.* **2018**, *99*, 1907–1924. [CrossRef]
25. Stewart, I.D.; Oke, T.R.; Krayenhoff, E.S. Evaluation of the 'local climate zone' scheme using temperature observations and model simulations. *Int. J. Climatol.* **2014**, *34*, 1062–1080. [CrossRef]
26. Tse, J.W.P.; Yeung, P.S.; Fung, J.C.H.; Ren, C.; Wang, R.; Wong, M.M.F.; Meng, C.A.I. Investigation of the meteorological effects of urbanization in recent decades: A case study of major cities in Pearl River Delta. *Urban Clim.* **2018**, *26*, 174–187. [CrossRef]

27. Gong, P.; Chen, B.; Li, X.; Liu, H.; Wang, J.; Bai, Y.; Chen, J.; Chen, X.; Fang, L.; Feng, S.; et al. Mapping essential urban land use categories in China (EULUC-China): Preliminary results for 2018. *Sci. Bull.* **2020**, *65*, 182–187. [CrossRef]

28. Bechtel, B.; Alexander, P.J.; Böhner, J.; Ching, J.; Conrad, O.; Feddema, J.; Mills, G.; See, L.; Stewart, I. Mapping Local Climate Zones for a Worldwide Database of the Form and Function of Cities. *ISPRS Int. J. Geo-Inf.* **2015**, *4*, 199–219. [CrossRef]

29. Brousse, O.; Martilli, A.; Foley, M.; Mills, G.; Bechtel, B. WUDAPT, an efficient land use producing data tool for mesoscale models? Integration of urban LCZ in WRF over Madrid. *Urban Clim.* **2016**, *17*, 116–134. [CrossRef]

30. Liu, X.; Huang, Y.; Xu, X.; Li, X.; Li, X.; Ciais, P.; Lin, P.; Gong, K.; Ziegler, A.D.; Chen, A.; et al. High-spatiotemporal-resolution mapping of global urban change from 1985 to 2015. *Nat. Sustain.* **2020**, *3*, 564–570. [CrossRef]

31. Li, Z.; Wan, B.; Zhou, Y.; Wong, H. Incoming data quality control in high-resolution urban climate simulations: A Hong Kong–Shenzhen area urban climate simulation as a case study using the WRF/Noah LSM/SLUCM model (Version 3.7.1). *Geosci. Model Dev.* **2020**, *13*, 6349–6360. [CrossRef]

32. Sun, Y.; Zhang, N.; Miao, S.; Kong, F.; Zhang, Y.; Li, N. Urban Morphological Parameters of the Main Cities in China and Their Application in the WRF Model. *J. Adv. Model. Earth Syst.* **2021**, *13*, e2020MS002382. [CrossRef]

33. Stewart, I.D.; Oke, T.R. Local climate zones for urban temperature studies. *Bull. Am. Meteorol. Soc.* **2012**, *93*, 1879–1900. [CrossRef]

34. Johnson, B.A.; Jozdani, S.E. Local Climate Zone (LCZ) Map Accuracy Assessments Should Account for Land Cover Physical Characteristics that Affect the Local Thermal Environment. *Remote Sens.* **2019**, *11*, 2420. [CrossRef]

35. Bechtel, B.; Alexander, P.J.; Beck, C.; Böhner, J.; Brousse, O.; Ching, J.; Demuzere, M.; Fonte, C.; Gál, T.; Hidalgo, J.; et al. Generating WUDAPT Level 0 data—Current status of production and evaluation. *Urban Clim.* **2019**, *27*, 24–45. [CrossRef]

36. Kotharkar, R.; Bagade, A. Local Climate Zone classification for Indian cities: A case study of Nagpur. *Urban Clim.* **2017**, *24*, 369–392. [CrossRef]

37. Zheng, Y.; Ren, C.; Xu, Y.; Wang, R.; Ho, J.; Lau, K.; Ng, E. GIS-based mapping of Local Climate Zone in the high~density city of Hong Kong. *Urban Clim.* **2017**, *24*, 419–448. [CrossRef]

38. Lelovics, E.; Unger, J.; Gál, T.; Gál, C.V. Design of an urban monitoring network based on Local Climate Zone mapping and temperature pattern modelling. *Clim. Res.* **2014**, *60*, 51–62. [CrossRef]

39. Wang, R.; Ren, C.; Xu, Y.; Lau, K.K.L.; Shi, Y. Mapping the local climate zones of urban areas by GIS-based and WUDAPT methods: A case study of Hong Kong. *Urban Clim.* **2018**, *24*, 567–576. [CrossRef]

40. Bechtel, B.; Daneke, C. Classification of Local Climate Zones Based on Multiple Earth Observation Data. *IEEE J. Sel. Top. Appl. Earth Obs. Remote Sens.* **2012**, *5*, 1191–1202. [CrossRef]

41. Wang, C.; Middel, A.; Myint, S.W.; Kaplan, S.; Brazel, A.J.; Lukasczyk, J. Assessing local climate zones in arid cities: The case of Phoenix, Arizona and Las Vegas, Nevada. *ISPRS J. Photogramm. Remote. Sens.* **2018**, *141*, 59–71. [CrossRef]

42. He, S.; Zhang, Y.; Gu, Z.; Su, J. Local climate zone classification with different source data in Xi'an, China. *Indoor Built Environ.* **2019**, *28*, 1190–1199. [CrossRef]

43. Demuzere, M.; Bechtel, B.; Middel, A.; Mills, G. Mapping Europe into local climate zones. *PLoS ONE* **2019**, *14*, e0214474. [CrossRef] [PubMed]

44. Fonte, C.C.; Lopes, P.; See, L.; Bechtel, B. Using OpenStreetMap (OSM) to enhance the classification of local climate zones in the framework of WUDAPT. *Urban Clim.* **2019**, *28*, 100456. [CrossRef]

45. Ren, C.; Cai, M.; Li, X.; Zhang, L.; Wang, R.; Xu, Y.; Ng, E. Assessment of Local Climate Zone Classification Maps of Cities in China and Feasible Refinements. *Sci. Rep.* **2019**, *9*, 1–11. [CrossRef]

46. Bechtel, B.; See, L.; Mills, G.; Foley, M. Classification of Local Climate Zones Using SAR and Multispectral Data in an Arid Environment. *IEEE J. Sel. Top. Appl. Earth Obs. Remote Sens.* **2016**, *9*, 3097–3105. [CrossRef]

47. Ma, Q.; Wang, Y.W.; Miao, S.G.; Zhang, Y.; Mu, Q. Study on construction of land use classification datasets with building type in large cities of China. *Trans. Atmos. Sci.* **2022**, *45*, 135–147.

48. Verdonck, M.L.; Okujeni, A.; van der Linden, S.; Demuzere, M.; De Wulf, R.; Van Coillie, F. Influence of neighbourhood information on 'Local Climate Zone'mapping in heterogeneous cities. *Int. J. Appl. Earth Obs. Geoinf.* **2017**, *62*, 102–113.

49. Shi, L.; Ling, F. Local Climate Zone Mapping Using Multi-Source Free Available Datasets on Google Earth Engine Platform. *Land* **2021**, *10*, 454. [CrossRef]

50. Zhu, X.X.; Hu, J.; Qiu, C.; Shi, Y.; Kang, J.; Mou, L.; Bagheri, H.; Häberle, M.; Hua, Y.; Wang, Y.; et al. So2Sat LCZ42: A Benchmark Dataset for Global Local Climate Zones Classification. *IEEE Geosci. Remote Sens. Mag.* **2015**, *14*, 8.

51. Ren, C.; Wang, R.; Cai, M.; Xu, Y.; Zheng, Y.; Ng, E. The accuracy of LCZ maps generated by the world urban database and access portal tools (WUDAPT) method: A case study of Hong Kong. In Proceedings of the The Fourth International Conference on Urban Hot Island Countermeasures, Singapore, 30 May–1 June 2016.

52. Kim, M.; Jeong, D.; Kim, Y. Local climate zone classification using a multi-scale, multi-level attention network. *ISPRS J. Photogramm. Remote Sens.* **2021**, *181*, 345–366. [CrossRef]

53. McRae, I.; Freedman, F.R.; Rivera, A.; Li, X.; Dou, J.; Cruz, I.; Ren, C.; Dronova, I.; Fraker, H.; Bornstein, R. Integration of the WUDAPT, WRF, and ENVI-met models to simulate extreme daytime temperature mitigation strategies in San Jose, California. *Build. Environ.* **2020**, *184*, 107180. [CrossRef]

54. Mushore, T.D.; Dube, T.; Manjowe, M.; Gumindoga, W.; Chemura, A.; Rousta, I.; Odindi, J.; Mutanga, O. Remotely sensed retrieval of Local Climate Zones and their linkages to land surface temperature in Harare metropolitan city, Zimbabwe. *Urban Clim.* **2019**, *27*, 259–271. [CrossRef]

55. Cai, M.; Ren, C.; Xu, Y.; Dai, W.; Wang, X.M. Local Climate Zone Study for Sustainable Megacities Development by Using Improved WUDAPT Methodology—A Case Study in Guangzhou. *Procedia Environ. Sci.* **2016**, *36*, 82–89. [CrossRef]

56. Cai, M.; Ren, C.; Xu, Y.; Lau, K.K.-L.; Wang, R. Investigating the relationship between local climate zone and land surface temperature using an improved WUDAPT methodology—A case study of Yangtze River Delta, China. *Urban Clim.* **2018**, *24*, 485–502. [CrossRef]

57. Wang, R.; Cai, M.; Ren, C.; Bechtel, B.; Xu, Y.; Ng, E. Detecting multi-temporal land cover change and land surface temperature in Pearl River Delta by adopting local climate zone. *Urban Clim.* **2019**, *28*, 100455. [CrossRef]

58. Shi, Y.; Ren, C.; Lau, K.K.-L.; Ng, E. Investigating the influence of urban land use and landscape pattern on PM2.5 spatial variation using mobile monitoring and WUDAPT. *Landsc. Urban Plan.* **2019**, *189*, 15–26. [CrossRef]

59. Mouzourides, P.; Eleftheriou, A.; Kyprianou, A.; Ching, J.; Neophytou, M.K.-A. Linking local-climate-zones mapping to multi-resolution-analysis to deduce associative relations at intra-urban scales through an example of Metropolitan London. *Urban Clim.* **2019**, *30*, 100505. [CrossRef]

60. Khamchiangta, D.; Dhakal, S. Future urban expansion and local climate zone changes in relation to land surface temperature: Case of Bangkok Metropolitan Administration, Thailand. *Urban Clim.* **2021**, *37*, 100835. [CrossRef]

61. Xu, Y.; Ren, C.; Cai, M.; Wang, R. Issues and challenges of remote sensing-based local climate zone mapping for high-density cities. In Proceedings of the 2017 Joint Urban Remote Sensing Event (JURSE), Dubai, United Arab Emirates, 6–8 March 2017; IEEE: New York City, NY, USA; pp. 1–4.

62. Demuzere, M.; Kittner, J.; Martilli, A.; Mills, G.; Moede, C.; Stewart, I.D.; van Vliet, J.; Bechtel, B. A global map of local climate zones to support earth system modelling and urban-scale environmental science. *Earth Syst. Sci. Data* **2022**, *14*, 3835–3873. [CrossRef]

63. Yoo, C.; Han, D.; Im, J.; Bechtel, B. Comparison between convolutional neural networks and random forest for local climate zone classification in mega urban areas using Landsat images. *ISPRS J. Photogramm. Remote Sens.* **2019**, *157*, 155–170. [CrossRef]

64. Zheng, J.; Zhao, Y.; Wu, W.; Chen, M.; Li, W.; Fu, H. Partial Domain Adaptation for Scene Classification From Remote Sensing Imagery. *IEEE Trans. Geosci. Remote Sens.* **2023**, *61*, 5601317. [CrossRef]

65. Zheng, J.; Wu, W.; Yuan, S.; Zhao, Y.; Li, W.; Zhang, L.; Dong, R.; Fu, H. A Two-Stage Adaptation Network (TSAN) for Remote Sensing Scene Classification in Single-Source-Mixed-Multiple-Target Domain Adaptation (S^2M^2T DA) Scenarios. *IEEE Trans. Geosci. Remote Sens.* **2022**, *60*, 5609213. [CrossRef]

66. Abdelkader, M.; Temimi, M.; Colliander, A.; Cosh, M.H.; Kelly, V.R.; Lakhankar, T.; Fares, A. Assessing the Spatiotemporal Variability of SMAP Soil Moisture Accuracy in a Deciduous Forest Region. *Remote Sens.* **2022**, *14*, 3329. [CrossRef]

67. Liu, S.; Shi, Q. Local climate zone mapping as remote sensing scene classification using deep learning: A case study of metropolitan China. *ISPRS J. Photogramm. Remote Sens.* **2020**, *164*, 229–242. [CrossRef]